Composites Part B 224 (2021) 109177

Contents lists available at ScienceDirect

Composites Part B

journal homepage: www.elsevier.com/locate/composites

Enhancement of Mode I fracture toughness properties of epoxy reinforced with graphene nanoplatelets and carbon nanotubes

Nishant Shirodkar [a,*], Shengfeng Cheng [b], Gary D. Seidel [a,*]

[a] Kevin T. Crofton Aerospace and Ocean Engineering Department, Virginia Polytechnic Institute and State University, Blacksburg, VA 24061, USA
[b] Department of Physics and Center for Soft Matter and Biological Physics, affiliated with Macromolecules Innovation Institute and Department of Mechanical Engineering, Virginia Tech, Blacksburg, VA 24061, USA

ARTICLE INFO

Keywords:
Carbon nanotubes
Graphene nanoplatelets
Fracture toughness
Reinforced epoxy
Scanning electron microscopy (SEM)
Nano composites

ABSTRACT

Relative to the conventional metals used in structures, epoxy-based composites have poor fracture toughness properties. This has long been a weak link when using epoxy composites for structural applications and therefore several efforts are being made to improve their fracture toughness. In this experimental study, the enhancement of fracture toughness brought about by the addition of carbon nanotubes (CNTs) and graphene nanoplatelets (GNPs) was investigated. CNT-Epoxy and GNP-Epoxy Compact Tension (CT) samples were fabricated with 0.1% and 0.5% nanofiller weight concentrations. The potential synergistic effects of dual nanofiller reinforcements were also explored using CNT/GNP-Epoxy CT samples at a 1:1 ratio of CNT:GNP. Displacement controlled CT tests were conducted according to ASTM D5045 test procedure and the critical stress intensity factor, K_{IC}, and the critical fracture energy, G_{IC}, were calculated for all the material systems. Significant enhancements relative to neat epoxy were observed in reinforced epoxies. The CNT-Epoxy samples at 0.5% nanofiller concentration experienced the most enhancement with a $\sim$ 118% and $\sim$ 311% increase in fracture toughness and fracture energy, respectively. The GNP-Epoxy and CNT/GNP-Epoxy samples also demonstrated significant enhancements relative to neat epoxy, but the enhancements are in general weaker than those of the CNT-Epoxy samples. Fracture surfaces were analyzed via scanning electron microscopy. Instances of CNT pullouts on the fracture surface were observed, indicating the occurrence of crack bridging. Furthermore, increased surface roughness, an indicator of crack deflection, was observed along with some crack bifurcations in the GNP-Epoxy samples. A further exploration is needed to understand the poor synergy between CNTs and GNPs in the CNT/GNP-Epoxy samples, which may be due to the CNT:GNP ratio and particle sizes used in the current study.

1. Introduction

Carbon-based nanoparticles have spurred a lot of interest in the composites research area because of their excellent mechanical, thermal, and electrical properties, making them a very good choice as filler materials. Even at low weight concentrations, nanoparticles such as carbon nanotubes (CNTs) and graphene nanoplatelets (GNPs) enable significant enhancement of the matrix material's mechanical properties. Owing to their multifunctional capabilities, CNT and GNP reinforced nanocomposites have found applications in a variety of areas such as energy storage, structural composites, electrical packaging, and flexible electronics [1,2]. Structural composites, especially fiber reinforced polymer composites (FRPs) which consist of high strength carbon or glass fibers embedded in a weaker polymer matrix, are a key focus area for the application of CNTs and GNPs as they can be readily introduced into the binder during processing. Traditional FRPs suffer from several drawbacks such as weak interlaminar strength, fiber–matrix debonding, and poor fracture toughness properties. Compared with common metals such as steels, the fracture toughness of polymers is typically an order of magnitude lower [3]. Given that FRPs are typically less dense than metals, but have comparable stiffness and strength, establishing ways to systematically improve their fracture toughness will make them well rounded structural materials. In the past two decades, several efforts have been made towards enhancing the fracture toughness of FRPs, as well as polymer composites in general [4–8].

In efforts to improve the fracture properties of FRPs, key failure mechanisms such as inter-laminar delamination, fiber–matrix debonding, and matrix cracking have been identified. Methods such as interlayer stitching and ply-pinning are introduced to address the issue of delamination. Ravandi et al. investigated the effects of through-thickness stitching by applying flax and cotton stitches through flax

* Corresponding authors.
E-mail addresses: nish26@vt.edu (N. Shirodkar), gary.seidel@vt.edu (G.D. Seidel).

https://doi.org/10.1016/j.compositesb.2021.109177
Received 9 February 2021; Received in revised form 12 July 2021; Accepted 23 July 2021
Available online 29 July 2021

fiber/epoxy composite laminates [9]. The stitches act as bridging elements through the laminates and bridge the crack once it is initiated, thus lending it an added ability to resist crack growth. A 21% increase in fracture toughness was obtained by this method. In addition to delamination mitigation, methods to reduce fiber–matrix debonding have also been investigated. One natural thought is to increase the ability of the fibers to bond with the matrix for them to carry as much load as possible, thus disallowing crack growth and forming very strong crack bridging networks. Yildiz et al. grew CNTs on glass fibers and used these fuzzy fibers to improve fiber–matrix bonding [10]. A 113% increase in fracture toughness was observed. Several other works have explored similar techniques such as fuzzy carbon fibers and have found promising fracture toughness enhancements [11,12]. However, the processing involved in growing CNTs or other nanoscale features on fibers typically results in a strength penalty for the fibers, making them weaker than their unaltered counterparts [11,13]. A different reinforcing strategy involves strengthening the matrix material by incorporating additional rubbery or soft phases in the form of block copolymers. These softer phases endure much higher deformations than the surrounding brittle matrix, thereby slowing the advancement of cracks. Kamar et al. incorporated a triblock copolymer into carbon fiber reinforced epoxy polymer composites (CFRPs) to improve their mode-I fracture energy [14]. The copolymer, a triad of polystyrene–polybutadiene–polymethylmethacrylate, was used to modify the epoxy matrix. Samples with several phr (parts per hundred resin) concentrations were tested. It was observed that a copolymer concentration of 10 phr resulted in a 290% increase in fracture energy. Bakar et al. experimented with the addition of plasticizers to unsaturated polyester resins and studied its effect on the resulting materials' mechanical properties [15]. A 45% increase in fracture toughness was observed at a concentration of dioctyl phthalate of 5 phr. Despite the observed increase in fracture toughness brought about by the addition of copolymers, complexities and compatibility issues between the added copolymers and the matrix materials limit the applicable range of this approach [16–19].

Another method of reinforcing a matrix material involves dispersing small amounts of nanoparticles (carbon-based, metallic, etc.) in the matrix. Gojny et al. evaluated single-walled, double-walled, and multi-walled CNTs doped epoxy nanocomposites [6]. A maximum 43% increase in fracture toughness was observed for a nanocomposite reinforced with double-walled CNTs at 0.1% weight concentration. Kumar et al. investigated the enhancements caused by adding GNPs to epoxy and observed a ~200% increase in Mode I fracture toughness at 0.5% weight concentration [20]. Additional efforts have explored other nanoparticles based on silica, graphene, and copper, and zinc nanowires. Significant enhancements have been reported even with small amounts of nanofillers [5,7,8]. The approach of adding nanofillers has several advantages. First, a wide range of nanoparticles can be chosen to reinforce a certain polymer. Second, the low content of nanofillers that are needed for reinforcement only leads to a marginal change of the matrix weight, which is desirable in many applications. Finally, many nanofillers also possess other functionalities (e.g., electrical and thermal functions) in addition to mechanical reinforcement, thus lending the composite a multifunctional capability [21–30,30–48].

Fig. 1 is a compilation of various fracture toughness data for CNT-Epoxy, GNP-Epoxy and CNT/GNP-Epoxy nanocomposites obtained from the literature [6,16,20,49–64]. This plot highlights that while nanoparticle-reinforced epoxy composites have been studied to some extent, there is still no clear correlation revealed between the degree of enhancement and the concentration of CNTs and GNPs. The possible synergy between the two fillers is not well established and poorly understood. In this experimental study, we aim to systematically study the enhancement of material properties for epoxy-based composites at various nanofiller concentrations (0.1% and 0.5% in terms of weight) and a 1:1 mixing ratio of CNTs and GNPs. The underlying toughening mechanisms such as crack bridging, crack deflection, and crack branching are investigated. The reinforcing capabilities of CNTs, GNPs, and CNT/GNP mixtures as the nanofillers are quantified with neat epoxy as the baseline. Mode I fracture toughness properties are evaluated via Compact Tension (CT) tests and the critical stress intensity factor and fracture energy results are determined.

2. Experimental methodology

2.1. Materials

In this study, a two-part epoxy matrix material was used: EPON 862, a bisphenol-F resin, and EPIKURE Curing Agent W, an aromatic amine curing agent. Both resin and curing agent were supplied by Hexion. As reported by the manufacturer, the epoxy used has good performance characteristics, including low viscosity (2200 cP) at room temperature, low moisture absorption (2–2.5 wt%), and over 20 h of working life at room temperature. Pristine multi-walled CNTs (MWCNTs) were supplied by Nano-labs. The MWCNTs have a reported purity of >95% with some iron and sulfur residuals (the residual particle sizes ~ 80 nm), a reported outer diameter of 15 ± 5 nm and an inner diameter of 7 ± 2 nm, and an average length of 3 ± 2 μm. xGNP Grade H GNPs were supplied by XGSciences and have a reported average thickness ~ 15 nm and an average particle diameter of 5 μm. The GNP particles have a reported purity of over 95% with some residual acid contents. The CNTs and GNPs are not functionalized and are used in their pristine conditions for this study.

2.2. Fabrication

Positive counter molds were designed as per ASTM D5045 guidelines [65] and were 3D printed via a high-resolution Polyjet printer (Connex 3 Objet 500). Silicone molds were then prepared from the 3D printed template and used for the fabrication of CT samples. CNT and/or GNP doped epoxy nanocomposites with varying nanoparticle weight concentrations were fabricated to evaluate their effect on the fracture toughness properties of the reinforced epoxy. Table 1 lists the material compositions of the seven different material systems fabricated for this study. Neat epoxy samples (i.e. samples without any nanoparticle content) were fabricated by mixing the resin and curing agent at a ratio of 100:26.4 by weight, as prescribed by the manufacturer. After thorough mechanical mixing for approximately 10 min, the mixture was heated to 90 °C and maintained at that temperature to reduce its viscosity; it was simultaneously degassed at 90 kPa vacuum for 45 min. It has been noted in the literature that reduced viscosity aids in proper degassing [20]. The silicone molds were sprayed with a mold release agent and then the degassed mixture was poured into the molds. The samples were cured in an oven (MTI DZF-6020-HT) at 121 °C for 2 h and post cured at 176 °C for an additional 2 h.

To prepare nanocomposite samples, appropriate quantities (see Table 1) of the nanoparticles were measured in a glass beaker. Measured quantities of EPON 862 resin epoxy were added to the nanoparticles and the two were mixed using a high shear mixer at 2000 rpm for 45 min. During the high shear mixing process, the resin and nanoparticle mixture was held at 90 °C to reduce its viscosity and aid the nanoparticle diffusion. In order to further disperse the nanoparticles, the mixture was ultra-sonicated (QSonica Q500 A) in an ice-chilled water bath at 20 kHz and 30% amplitude for 10 min. After sonication, the required quantities of the curing agent were added and mixed with the resin–nanoparticle mixture using a high shear mixer at 2000 rpm for 10 min at room temperature. The resulting mixture was then degassed using the same parameters as for the neat epoxy samples. The subsequent processes for pouring the mixture in the molds and curing the samples were also consistent with the processes for the neat epoxy samples. The nanocomposite samples were fabricated in batches of five samples each for the seven different material systems.

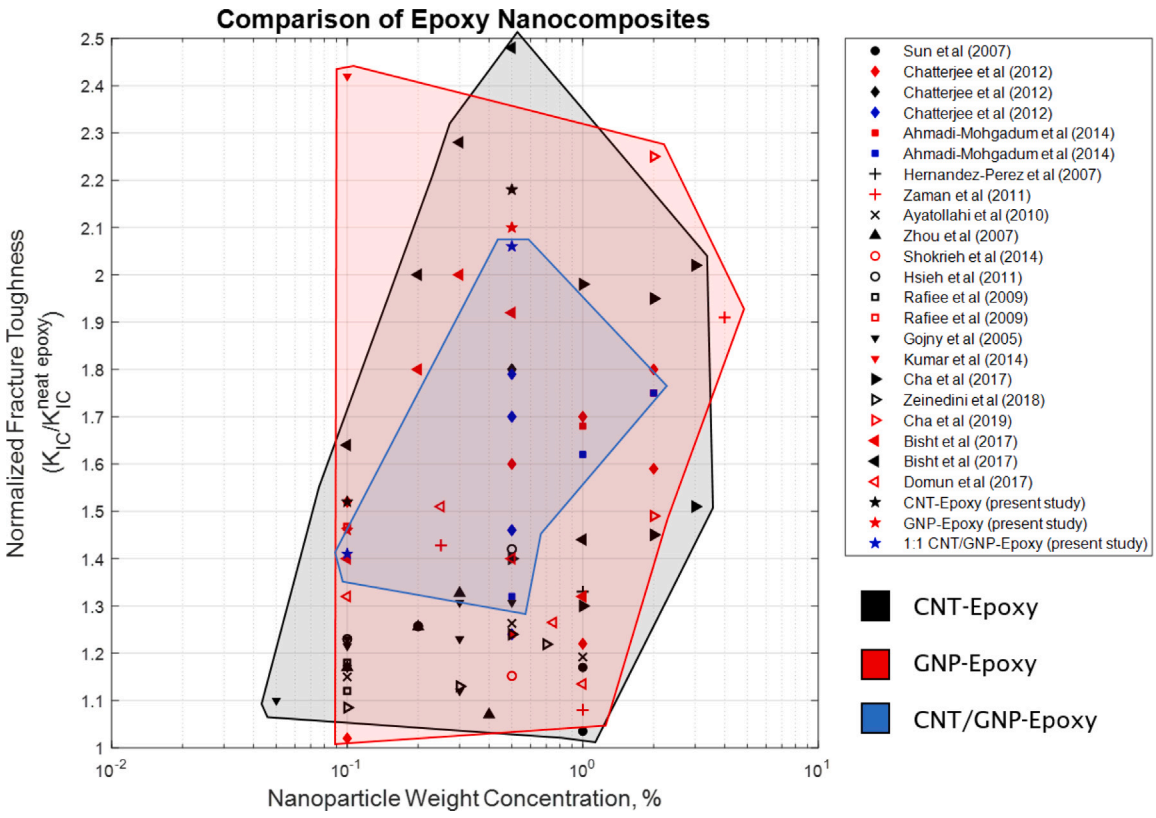

Fig. 1. Fracture toughness data for various CNT, GNP, and CNT/GNP-Epoxy nanocomposites, normalized by the value for neat epoxy, were collected from the literature and plotted against the nanofiller weight concentrations.

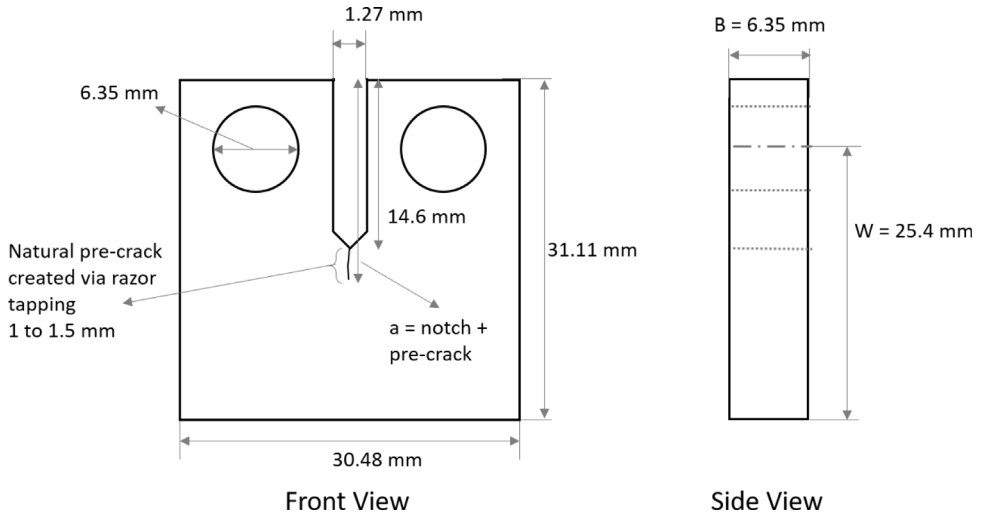

Fig. 2. Graphical illustration of the fabricated CT samples shown with their geometrical dimensions in millimeters (mm).

Table 1
Material compositions.

Material systems	CNTs, %wt	GNPs, % wt	Epoxy matrix, % wt
Neat Epoxy	0	0	100
0.1-CNT-Epoxy	0.1	0	99.9
0.1-GNP-Epoxy	0	0.1	99.9
0.1-CNT/GNP-Epoxy	0.05	0.05	99.9
0.5-CNT-Epoxy	0.5	0	99.5
0.5-GNP-Epoxy	0	0.5	99.5
0.5-CNT/GNP-Epoxy	0.25	0.25	99.5

2.3. Sample preparation

CT specimens were prepared according to ASTM D5045 standards [65] to evaluate the fracture toughness properties of the nanocomposites. Fig. 2 shows a graphical illustration of the CT samples with their geometric dimensions. The samples were cast using the silicone molds with a notch built into the mold. The thicknesses of the samples were within the prescribed ASTM guidelines such that a plane strain condition can be assumed at the crack tip. Additionally, raised features like the meniscus formation around the pin-holes and sample edges, an artifact of the casting process, were sanded to achieve a uniform thickness across the sample. Because of the limitations of

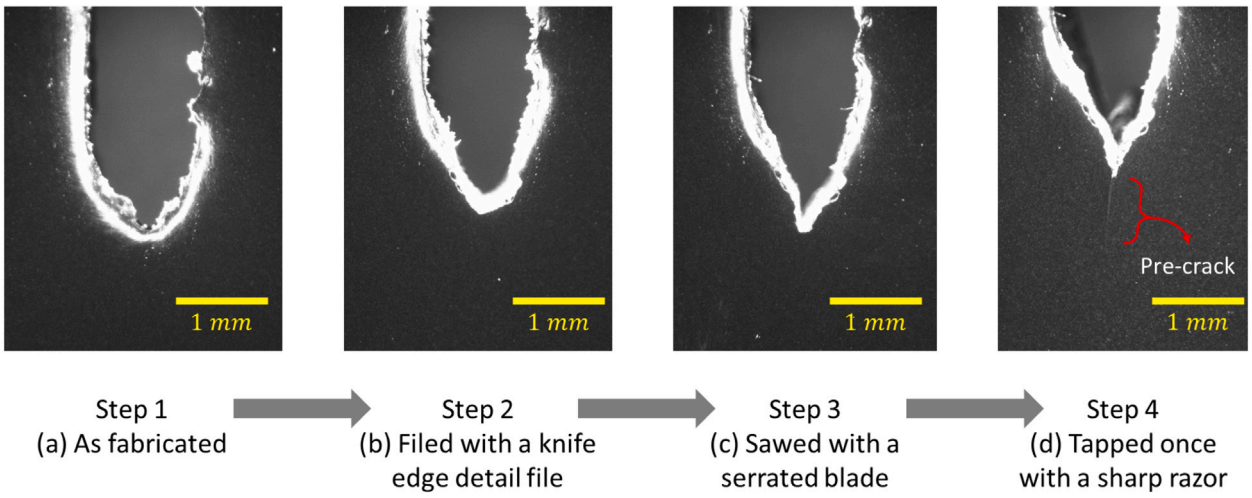

Fig. 3. Digital microscope images of a CT sample undergoing the process of notch-tip sharpening and pre-crack creation. Left to Right: cast sample, sample after filing, sample after sawing, and sample after razor blade tapping.

the casting process, the notch tip of the cast samples was not as sharp as required by ASTM standards. A sharp pre-crack is essential for a valid fracture toughness test because (a) a blunt crack tip results in a pseudo increase of the measured fracture toughness values [20] and (b) it violates the assumption of an ideal crack underlying linear elastic fracture mechanics (LEFM), the theory on which the calculations of the critical stress intensity factor, K_{IC}, and critical fracture energy, G_{IC}, are based [65,66]. To create a sharp pre-crack, ASTM guidelines were followed [65]. The cast sample's blunt notch tip was sharpened with a knife-edged file. The filed notch tip was sharpened further by sawing with a thin serrated blade. Finally, a sharp, natural pre-crack was initiated by tapping the notch tip with a razor blade. Fig. 3 shows images, acquired via digital microscopy, of a sample at every stage of the sharpening process of the notch tip and the creation of the pre-crack. In Fig. 3(d), the thin line extending beyond the machined notch tip is the sharp, natural pre-crack created by the razor blade tapping method.

2.4. Fracture toughness testing

Fracture toughness tests were conducted in an INSTRON universal double-columned test frame via a displacement controlled test at a displacement rate of 2 mm/min. The force, measured using a load cell, exerted on and the corresponding displacement of a sample were recorded until the sample failed. In this study, a sample was considered to be failed if the instantaneous load carrying capacity dropped by more than 80% from the peak load.[1] Through trial and error, it was observed that all samples cracked in half shortly upon meeting this criterion and hence, could be considered to be practically failed.[2] A batch of five samples for each material system was tested to account for the statistical variation in the load–displacement curves. The gathered data was analyzed and the peak load, fracture displacement, K_{IC}, and G_{IC} were calculated for every sample using the process outlined by ASTM standards.

[1] This study investigated the initiation fracture toughness of the materials and hence, the load and displacement data of the material past its peak load was not employed in the calculations of the fracture toughness values

[2] In some of the tested CNT-Epoxy samples, the crack did not propagate all the way through the sample despite registering a 80% load drop. However, the samples broke as they were being dismounted from the test fixture and hence, could be considered to be practically failed.

3. Results and discussion

3.1. Qualitative/visual assessments

Fig. 4 shows photographs of the fabricated CT samples. The addition of CNTs and/or GNPs lent a distinctive black hue to the composite samples as opposed to the nominally semi-transparent amber hue of the neat epoxy. Even at 0.1% weight concentration, there was a marked change in the color. At 0.5% weight concentration, increased opaqueness and a slightly darker black hue were observed. Some bubbles were observed around the outer edge of some samples (see Fig. 4). However, any samples with bubbles along the crack path— identified by inspecting the fracture surface after testing— were discarded and the corresponding data were excluded from the analysis.

3.2. Mechanical properties

Figs. 5(a–c) show the mean load–displacement curves for the CNT-Epoxy, GNP-Epoxy, and CNT/GNP-Epoxy nanocomposites, respectively, as well as the neat epoxy in each case as a reference. The plotted error bars represent data within two standard deviations of the mean. The load–displacement data has been post-processed and the value of displacement has been corrected according to ASTM D5045 procedures [65]. Specifically, the contribution from the initial non-linear loading regime, which can be attributed to sample compression, system compliance, and loading-pin penetration, has been subtracted from the measured raw value of displacement. The data in Fig. 5 therefore represents the linearized load–displacement curves, which are plotted using the slope of the linear part of a load–displacement curve, the peak load, and the corrected fracture displacement values.

The neat epoxy samples have an average peak load of 86.74 N and an average fracture displacement of 0.19 mm. These samples serve as a baseline for further comparisons. Adding 0.1% CNTs (by weight) to the epoxy resulted in ~53% increase in load-carrying capacity and ~36% increase in fracture displacement, with an average peak load of 132.09 N and average an fracture displacement of 0.26 mm. Increasing the CNT weight concentration to 0.5% led to ~120% increase in peak load (to 190.49 N) and ~89% increase in displacement (to 0.36 mm). For the GNP-Epoxy nanocomposite samples at 0.1% weight concentration, the peak load was enhanced by ~46% to 126.99 N and the fracture displacement was increased by ~32% to 0.25 mm. Increasing the GNP weight concentration to 0.5% makes the enhancement factor of the peak load and fracture displacement to be ~111% (to 182.70 N) and ~78% (to 0.34 mm), respectively. Nanocomposites reinforced with a

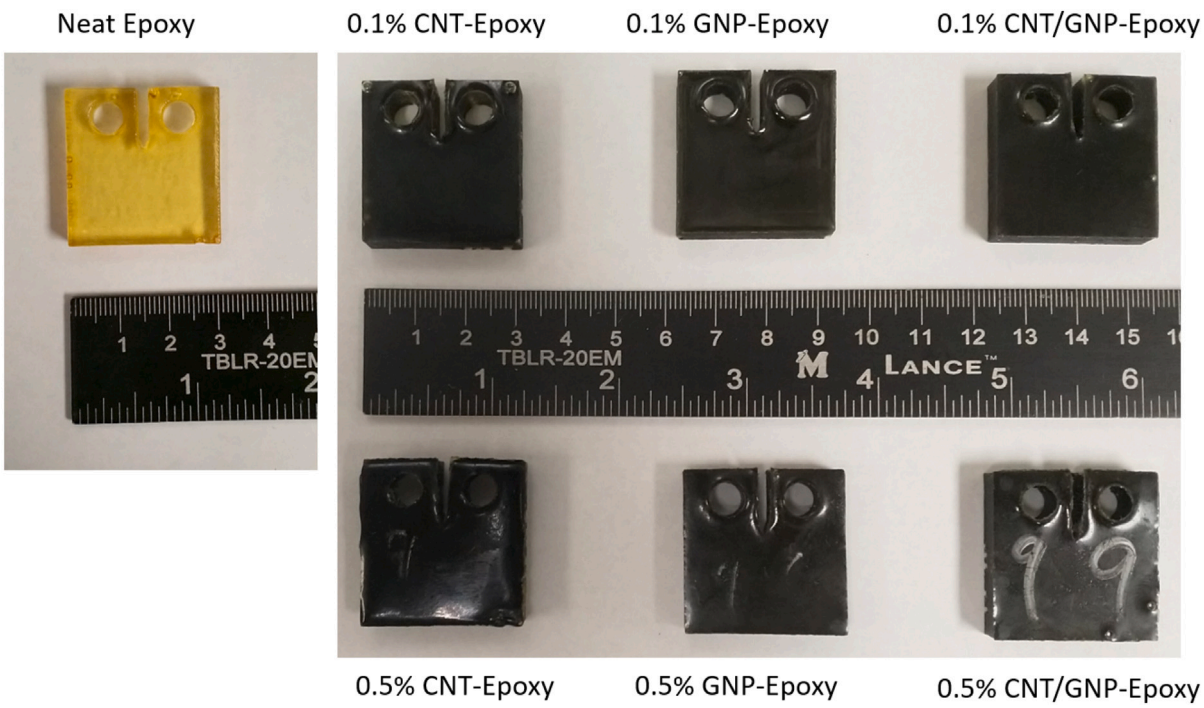

Fig. 4. Photographs of representative CT samples of the seven material systems fabricated for this study.

Table 2
Peak loads and fracture displacements of all the material systems.

Material system	Peak load (N)	% Increase	Fracture displacement (mm)	% Increase
Neat Epoxy	86.74 ± 5.04	–	0.19 ± 0.01	–
0.1-CNT-Epoxy	132.09 ± 2.86	~53	0.26 ± 0.003	~36
0.1-GNP-Epoxy	126.99 ± 6.01	~46	0.25 ± 0.01	~32
0.1-CNT/GNP-Epoxy	122.84 ± 8.32	~41	0.24 ± 0.01	~26
0.5-CNT-Epoxy	190.49 ± 6.94	~120	0.36 ± 0.01	~89
0.5-GNP-Epoxy	182.7 ± 5.91	~111	0.34 ± 0.01	~78
0.5-CNT/GNP-Epoxy	179.4 ± 4.97	~108	0.35 ± 0.01	~84

mixture of nanofillers are also of interest as synergistic effects may occur between nanofillers with different geometrical characteristics. CNTs and GNPs offer a good opportunity to explore such effects as CNTs are filament-like, while GNPs have a platelet shape. The different aggregation behavior among CNTs and GNPs may lead to new reinforcement mechanisms not involved in nanocomposites based on one type of nanofillers. For the CNT/GNP-Epoxy samples at 0.1% weight concentration and 1:1 weight ratio of CNT:GNP, the peak load was increased by ~41% to 122.84 N and the fracture displacement was increased by ~26% to 0.24 mm. When the weight concentration of the CNT/GNP mixture was increased to 0.5%, the peak load and fracture displacement were enhanced further, by ~108% to 179.40 N for the former and ~84% to 0.35 mm for the latter. Table 2 summarizes the average peak loads and fracture displacements of all the material systems tested, with the degree of enhancement quantified using the neat epoxy as a reference. The data are presented with the associated error bars (representing one standard deviations of the mean) to indicate the extent of variability or repeatability of the data from CT tests. It should be noted that the peak load value is not the indicator of a material's tensile strength, but rather its maximum load-carrying capacity in the presence of a crack. In other words, it represents the maximum amount of load a material can bear before a crack is able to grow in it and eventually lead to its failure.

As a straight comparison, the average peak loads and fracture displacements are also shown as bar plots in Fig. 6. It shows that the addition of CNTs, GNPs, and CNT/GNP mixtures to an epoxy matrix enhances its mechanical properties to resist fracture. The enhancement is more significant at 0.5% weight concentration of the nanofillers than at 0.1% weight concentration. At a given weight concentration, CNTs slightly outperforms GNPs, while both lead to enhancements marginally stronger than the CNT/GNP mixtures. The only exception is the fracture displacement of the CNT/GNP-Epoxy sample at 0.5% weight concentration, which is slightly larger than that of the GNP-Epoxy sample at the same weight concentration.

3.3. Fracture toughness and fracture energy

To further quantify the initiation fracture toughness of the nanocomposites studied here, Mode I critical stress intensity factor, K_{IC}, was calculated using Eq. (1), where P is the peak load, B is the average sample thickness, W is the specimen width as defined by ASTM D5045, and $f(x)$ is an empirical calibration factor dependent on crack length, a, and specimen width, W of each sample. Eq. (2) shows the formula for $f(x)$ where $x = a/W$.

$$K_{IC} = \frac{P}{BW^{1/2}} f(x) \tag{1}$$

$$f(x) = \frac{(2+x)(0.886 + 4.64x - 13.32x^2 + 14.72x^3 - 5.6x^4)}{(1-x)^{3/2}} \tag{2}$$

Using Eq. (1) the value of K_{IC} was found to be 0.75±0.04 MPa · $m^{1/2}$ and is consistent with the manufacturer's reported value of 0.8 MPa · $m^{1/2}$ [67]. The values of K_{IC} were 1.14 MPa · $m^{1/2}$, 1.10 MPa · $m^{1/2}$, and 1.06 MPa · $m^{1/2}$ for the CNT, GNP, CNT-GNP reinforced epoxy at 0.1% weight concentration, corresponding to an enhancement factor

Table 3
Comparison of the critical stress intensity factor (K_{IC}) and fracture energy (G_{IC}) of all the material systems.

Material systems	K_{IC} (MPa · $m^{1/2}$)	% Increase	G_{IC} (J/m^2)	% Increase
Neat Epoxy	0.75 ± 0.04	–	247.4 ± 29.87	–
0.1-CNT-Epoxy	1.14 ± 0.02	~52	502.92 ± 16.27	~103
0.1-GNP-Epoxy	1.10 ± 0.05	~46	469.18 ± 39.69	~89
0.1-CNT/GNP-Epoxy	1.06 ± 0.07	~41	440.53 ± 49.10	~78
0.5-CNT-Epoxy	1.64 ± 0.059	~118	1017.6 ± 65.57	~311
0.5-GNP-Epoxy	1.58 ± 0.05	~110	923 ± 43.69	~273
0.5-CNT/GNP-Epoxy	1.55 ± 0.043	~106	927.14 ± 36.64	~275

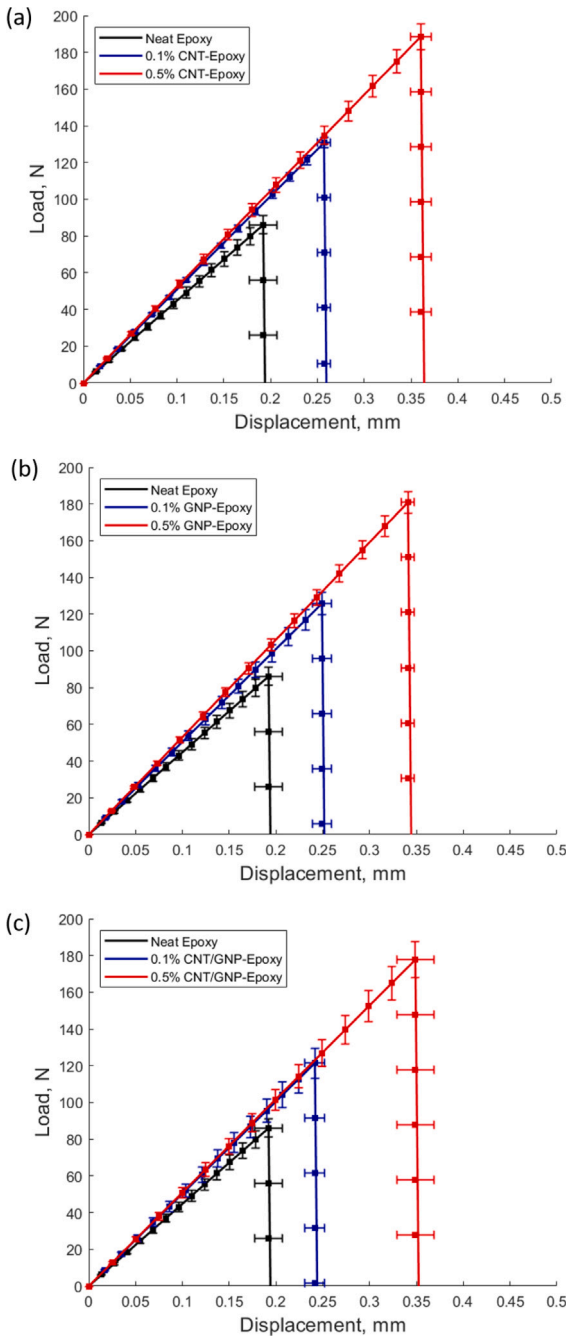

Fig. 5. Linearized load–displacement curves for (a) 0.1% and 0.5% CNT-Epoxy, (b) 0.1% and 0.5% GNP-Epoxy, and (c) 0.1% and 0.5% CNT/GNP-Epoxy. The result for the neat epoxy is included in each plot as a baseline. Error bars represent two standard deviations of the mean.

of 52%, 46%, and 41% with respect to the neat epoxy, respectively. At 0.5% weight concentration, CNT-Epoxy, GNP-Epoxy, and CNT/GNP-Epoxy samples achieved a ~118% (to 1.64 MPa · $m^{1/2}$), ~110% (to 1.58 MPa · $m^{1/2}$) and ~106% (to 1.55 MPa · $m^{1/2}$) increase in fracture toughness. Table 3 summarizes the average K_{IC} values and the associated error bars, corresponding to one standard deviation, for all the material systems tested. Compared with the neat epoxy, the reinforced samples showed a marked increase in initiation fracture toughness, even at a weight concentration as low as 0.1%.

Mode I critical fracture energy was calculated using Eq. (3), where U is the corrected strain energy (i.e. the area under the linearized load–displacement curve), B is the average sample thickness, W is the specimen width, and $\phi(x)$ is an empirical energy calibration factor. The expression for $\phi(x)$ is given in Eq. (4) (see Box I).

The value of G_{IC} was determined to be 247.4 J/m^2 for the baseline neat epoxy samples. For the reinforced samples at 0.1% weight concentration of the nanofillers, the fracture energy was increased by ~103% (to 502.92 J/m^2) for CNT-Epoxy, ~89% (to 469 J/m^2) for GNP-Epoxy. and ~78% (to 440.53 J/m^2) for the CNT/GNP-Epoxy samples. At the higher weight concentration of 0.5%, the CNT-Epoxy, GNP-Epoxy, and CNT/GNP-Epoxy samples exhibited an increase in fracture energy by ~311% (to 1017.6 J/m^2), ~273% (to 923 J/m^2) and ~275% (to 927.14 J/m^2), respectively. Table 3 summarizes all the average G_{IC} values and the associated error bars. The possible mechanisms underlying the observed enhancements of the fracture properties of the reinforced materials will be discussed later in the paper.

A direct comparison of fracture toughness (K_{IC}) and fracture energy (G_{IC}) is included in Fig. 7 as bar plots. Similar trends as those in Fig. 6 are observed. Enhancements of K_{IC} and G_{IC} are found for all the reinforced samples. For the reinforced composites containing the same fraction of nanofillers in terms of weight, CNTs perform the best, followed by GNPs, while the CNT/GNP mixtures exhibit an enhancement slightly weaker than both CNTs and GNPs. In other words, there appears to be no synergy among CNTs and GNPs as reinforcement agents. However, this may be due to the 1:1 mass ratio between the two nanofillers used in the mixtures in this study. The connection between mass ratio and possible synergistic effects in CNT/GNP mixtures needs to be explored with more studies.

3.4. Fracture surface analysis

Scanning Electron Microscopy (SEM) was used to image the post-failure surfaces of the fractured samples and some results were included in Fig. 8. These images were taken at a magnification of 500x. The neat epoxy samples exhibit smooth surfaces, with almost no features or roughness after fracture, which indicates unobstructed crack propagation after initiation (Fig. 8(a)). In comparison, the CNT-Epoxy samples, at both 0.1% and 0.5% nanofiler weight concentrations, have visible clusters of CNTs on the fracture surface (Fig. 8(b)). Minor surface roughness near the clusters is also observed. In Figs. 9(a-ii, a-iii) where the fracture surfaces were imaged at higher magnifications (5000x and 20,000x), CNTs are clearly visible and the epoxy has impregnated the CNT clusters quite well. Instances of CNT pullouts are also observed, indicating crack bridging across the fracture surface. Further, it is

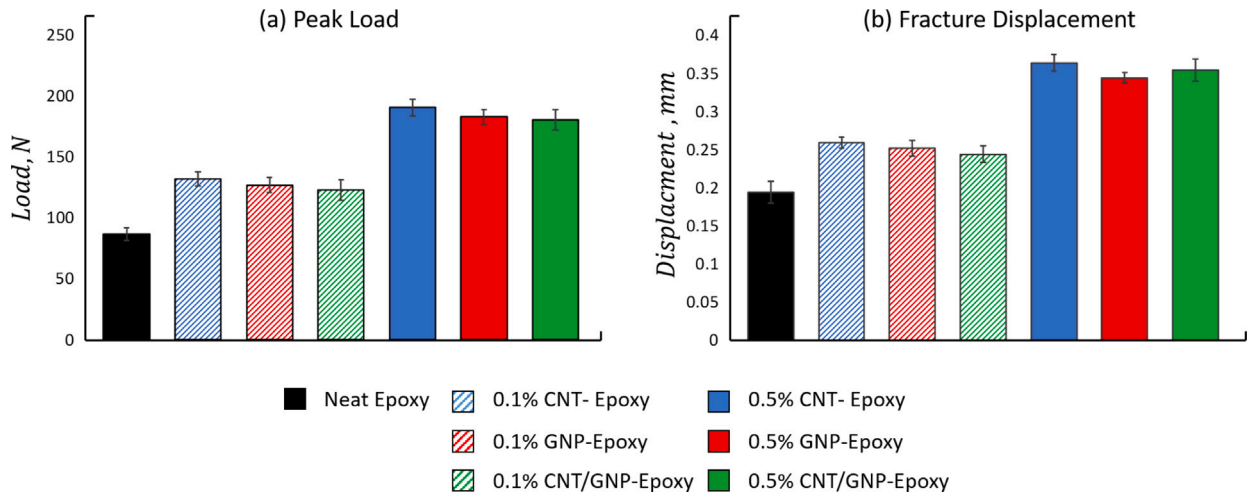

Fig. 6. Bar plots comparing (a) average peak load and (b) fracture displacement for the seven material systems. Error bars shown over every bar represent two standard deviations of the mean.

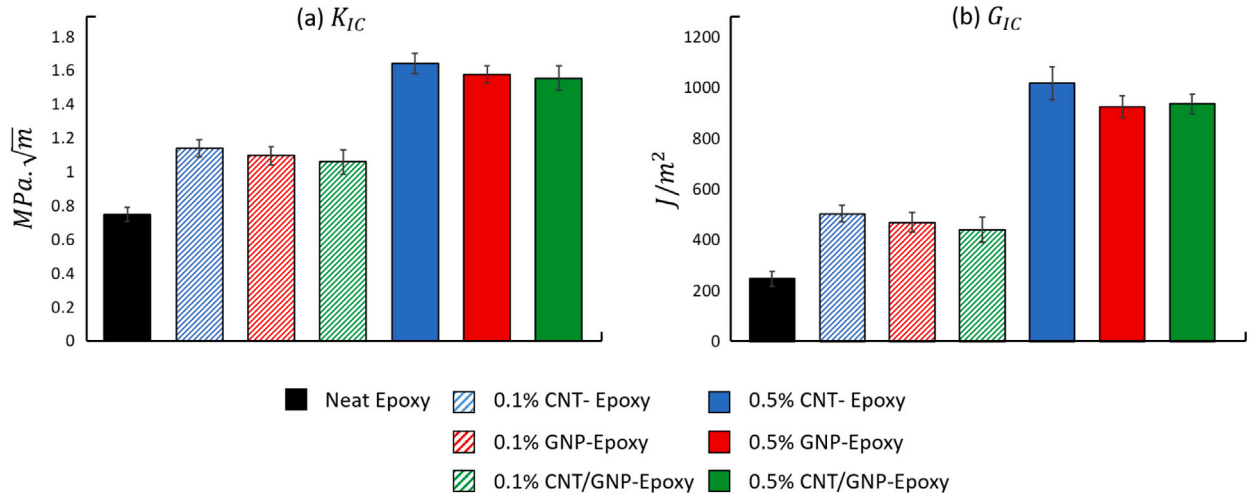

Fig. 7. Bar plots comparing (a) fracture toughness (K_{IC}) and (b) fracture energy (G_{IC}) for the seven material systems. Error bars represent two standard deviations of the mean.

$$G_{IC} = \frac{U}{BW\phi(x)} \tag{3}$$

$$\phi = \frac{(1.91 + 19.11x - 2.51x^2 - 23.22x^3 + 20.54x^4)(1-x)}{(19.11 + 5.02x - 69.67x^2 + 82.12x^3)(1-x) + 2(1.91 + 19.11x - 2.51x^2 - 23.22x^3 + 20.54x^4)} \tag{4}$$

Box I.

believed that the wavy nature of the CNTs observed in Figs. 9(a-iii, c-iii) can lead to mechanical interlocking behavior, thereby making CNT pullouts difficult and resulting in stronger crack bridging elements.

Compared with the CNT-Epoxy samples, the GNP-Epoxy samples have visibly more surface roughness, as seen in Figs. 8(c-i, c-ii). The two dimensional GNPs are much stronger and stiffer than the surrounding epoxy. Thus, it is energetically favorable for an advancing crack front to deviate around GNPs, rather than go through them. In this sense, the embedded GNPs act as barriers to obstruct the advancement of cracks. The resulting crack deviation or deflection creates rough surface features in its wake. Such roughness has been observed by others who have also attributed it to crack deflection [68,69]. The fracture surface was found to be rougher as the nanofiller weight concentration was increased to 0.5%; this is indicative of more crack deflection occurring along the crack path. It must be noted that as a crack circumvents a GNP, it may conceal a GNP under the fracture surface, which makes spotting GNPs via SEM harder than detecting CNTs. A few instances of partially exposed GNPs are visible in Figs. 9(b-ii,iii), wherein cracks can be seen bifurcating and deflecting around the GNPs.

SEM images of the fractured surfaces of the CNT/GNP-Epoxy samples shown in Figs. 9(c-i, c-ii, c-iii) reveal markers indicating the occurrence of both crack mitigation processes: deflection and bridging. The former can be deduced from the increased surface roughness and the latter is confirmed by the presence of CNT clusters and pullouts on the fractured surfaces [68,69]. Fig. 9(c-iii) shows an instance of CNTs agglomerated around/near a GNP (most likely a group of GNPs situated close to each other). Exposed pulled-out CNTs are visible in front of the bifurcation point of the crack, suggesting that both crack bridging and

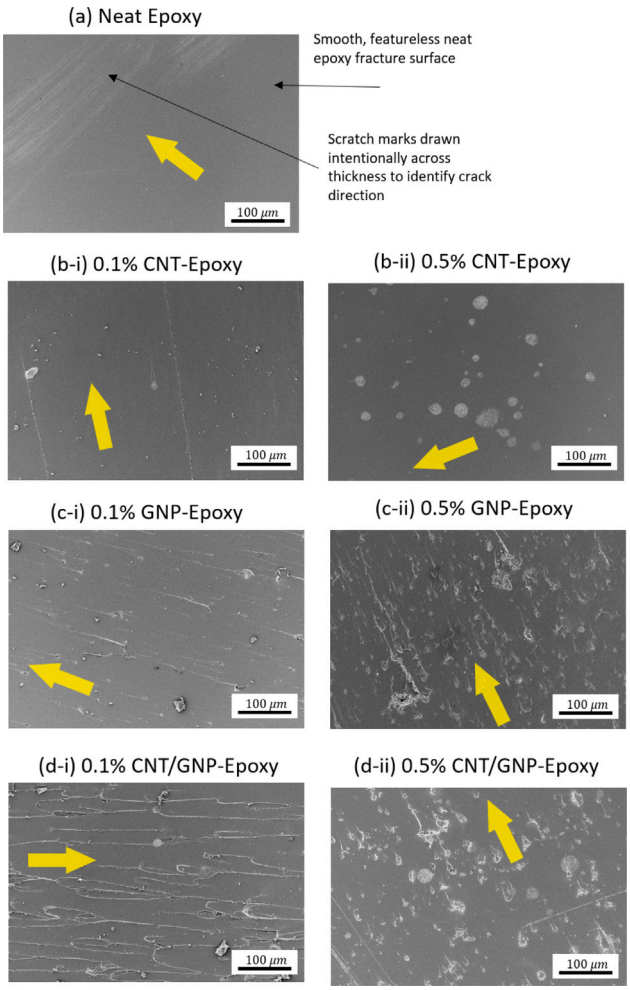

Fig. 8. SEM images of the fracture surfaces of all the tested materials: (a) Neat Epoxy, (b-i, ii) 0.1% and 0.5% CNT-Epoxy, (c-i, ii) 0.1% and 0.5% GNP-Epoxy, (d-i, ii) 0.1% and 0.5% CNT/GNP-Epoxy. In each image, the direction of the yellow arrow indicates the direction of crack propagation.

deflection may have occurred in that region. Furthermore, SEM images shown in Fig. 8(d-i, d-ii) also reveal that as the weight concentration of the nanofillers is increased, the fractured surface becomes rougher and more CNT clusters can be observed on the surface.

3.5. Discussion on toughening mechanisms

CNT, GNP, and CNT/GNP reinforced epoxies experience different dominant toughening mechanisms due to characteristics such as different geometry (fiber-like for CNTs as opposed to plate-like for GNPs), aspect ratio, and available surface area to form interfaces with the epoxy matrix. Furthermore, the active mechanisms involved in enhancing initiation fracture toughness are different from those mitigating crack propagation. CNTs and GNPs are much stiffer and stronger than the surrounding epoxy matrix and as a result, the localized stiffness of the region ahead of the crack front is higher. This influences the elastic and inelastic stress distributions in the fracture process zone (FPZ) ahead of the crack tip, which in turn affects the size of the FPZ of the material [70,71]. The initiation fracture toughness of a material is related to the radius of the FPZ; larger FPZs result in higher initiation fracture toughness [71]. In addition, the orientation of the nanofillers present in the localized matrix region also affects the local stiffness, thereby affecting the FPZ. CNTs and GNPs that lie parallel with the direction of loading (Mode I opening loads) increase the stiffness in that direction. Therefore, in a randomly oriented dispersion of nanofillers, a certain percentage of the total individual nanofillers take a favorable orientation and increase the local stiffness in the Mode I loading direction. This also affects the FPZ size ahead of the crack front and is believed to contribute towards the initiation toughness enhancement observed in the epoxy nanocomposites.

Due to differences in the size of GNPs and CNTs used in this study, it can be shown that at the same weight there are more CNTs than GNPs by about 1 order of magnitude.[3] With more individual CNTs than individual GNPs, there is a greater possibility for favorably aligned CNTs which enhance the stiffness in the Mode I direction. Similarly, GNPs that are favorably aligned with the loading direction can use their 2D plane stiffness to improve stiffness in the Mode 1 direction; however, there are fewer of them, and those that are lying parallel to the loading direction offer little improved stiffness from their through-thickness direction. The differences in the local stiffness resulting from the above mentioned phenomenon, and consequently their influence on the FPZ, explain the higher initiation toughness values of the CNT-Epoxy samples compared with their counterparts. It must be noted that CNT agglomerations impregnated with epoxy (observed in SEM images, Fig. 9(a-iii)) may impart some regions with stiffness enhancement larger than the individual CNTs which may aid the initiation toughness enhancement. Crack bridging and crack deflection are primary mechanisms that dominate the mitigation of crack propagation in CNT and GNP reinforced epoxies, respectively [6,72]. Crack bridging occurs in the wake of a crack tip and is a result of bridging elements present on the crack path, more specifically, across the separated fracture surfaces that lie in the wake of a crack (see Fig. 10(a)). The high aspect ratios of CNTs make them suitable for crack bridging. Load transfer occurs from the epoxy to the strong and stiff CNTs via interfaces held by van der Waals forces that exist between the CNTs and epoxy. During crack initiation under Mode I loading, the wake of the crack tends to open but is halted by the CNTs which act as bridging elements [73–76]. This, in turn, slows crack propagation [76]. In addition to the van der Waals forces between the CNTs and epoxy at the interface, there exists interfacial friction and some degree of mechanical interlocking between the CNTs and epoxy, both of which must be overcome for the CNTs to pull out and the crack to advance. The CNTs used in this study have random chirality, which results in wavy, convoluted profiles along the length of the CNTs (Fig. 9). Such complex waviness results in features resembling hooks and zigzag lines, which lead to strong mechanical interlocking. Such interlocking, coupled with interfacial friction, is believed to contribute towards increasing the ability of CNTs to bridge cracks [77–79]. Crack deflection typically occurs in the region ahead of the crack front; but, it still requires the crack to initiate and advance in order to deflect, and hence, is classified as a crack propagation mitigation mechanism. GNPs that lie ahead of a crack front effectively act as a wall because of their 2D planar structure. The localized stiffness of the GNP-Epoxy region ahead of the crack front is high, and thus, the crack path is forced to deviate around those regions (Fig. 10(b)). This process slows down crack propagation. The presence of pulled-out GNPs has been observed in the SEM images (Fig. 8(b-iii)) which suggests GNP pullout as an additional possible mechanism for crack propagation mitigation.

The CNT/GNP-Epoxy samples exhibit both toughening mechanisms, i.e., crack bridging and crack deflection. Chatterjee et al. explored the synergistic effects of CNTs and GNPs at different CNT/GNP ratios

[3] In the present study, the approximate diameter of a GNP is ~ 5 μm, while the CNTs have an average an outer diameter (OD) of ~ 15 nm. Considering that a CNT can be thought of as a GNP rolled into a tubular structure, a single GNP — assumed to be a 5 μm × 5 μm square plate for this hypothetical thought experiment — can yield about 10 multi-walled CNTs with ~ 5 μm length and ~ 15 nm OD. Therefore, for a CNT-Epoxy sample and a GNP-Epoxy sample at the same nanofiller weight concentration, there are more individual CNTs than individual GNPs dispersed in the epoxy.

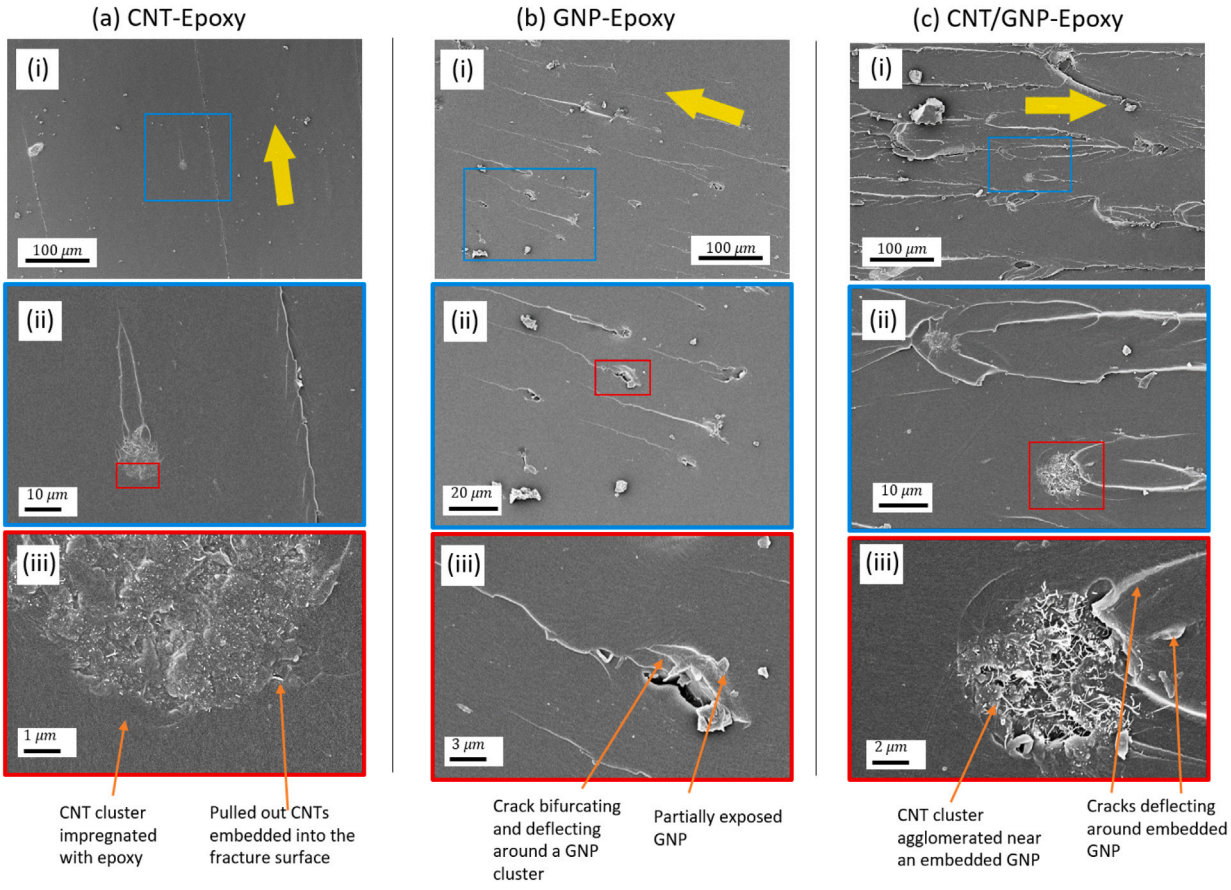

Fig. 9. Sequential high magnification SEM images of the fracture surfaces of (a) 0.1% CNT-Epoxy, (b) 0.1% GNP-Epoxy, (c) 0.1% CNT/GNP-Epoxy. The images in the top, middle, and bottom rows are taken at 500×, 5000×, and 20,000× magnification, respectively. Colored boxes highlight the approximate regions magnified further. In each image, the direction of the yellow arrow indicates the direction of crack propagation. (For interpretation of the references to color in this figure legend, the reader is referred to the web version of this article.)

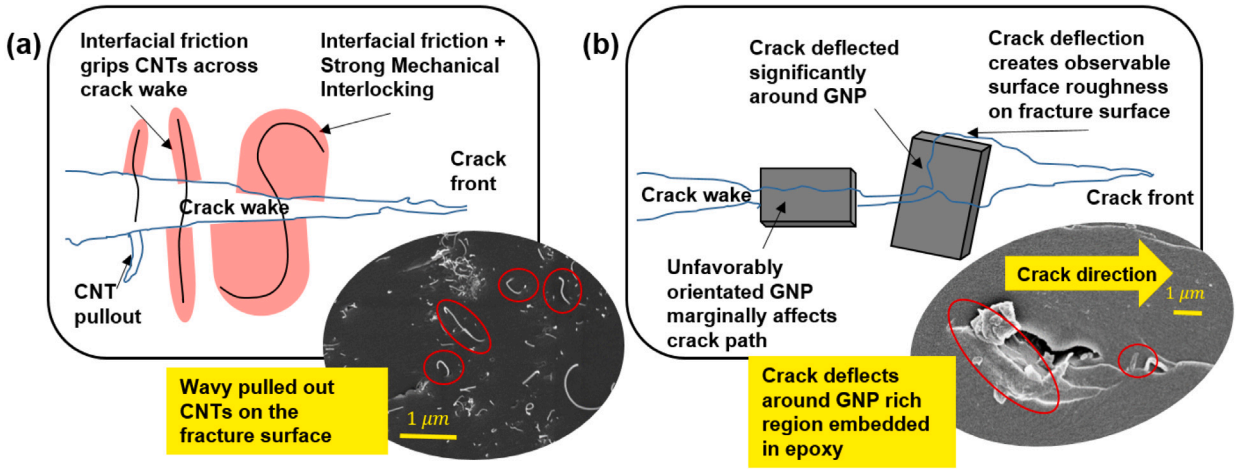

Fig. 10. Graphical illustrations of (a) CNTs bridging the fractured surface in the wake of a crack and the influence of mechanical interlocking in enhancing the CNTs' bridging capabilities; (b) GNPs deflecting cracks and the effects of GNP orientation on the efficacy of crack deflection. SEM micrographs are included to demonstrate the proposed toughening mechanisms.

and experimented with different particle sizes [72]. They reported that only the samples reinforced with CNT/GNP mixtures at the 9:1 ratio of CNT:GNP and 0.5% weight concentration exhibited enhancements larger than those of the CNT-Epoxy samples containing 0.5% CNTs by weight; at all other ratios (1:3, 1:5, 1:9, 5:1, and 3:1), the values of K_{IC} are smaller for the CNT/GNP-Epoxy samples. A similar trend is observed in the present study, where the CNT/GNP-Epoxy samples with CNT:GNP at the 1:1 ratio have relatively lower K_{IC} values than the CNT-Epoxy samples. At the 1:1 ratio, the weights of CNTs and GNPs are equal, however, there are more individual CNTs than individual GNPs, as discussed earlier. When 50% of the CNTs in a CNT-reinforced sample are replaced with GNPs, the total number of nanofillers is reduced roughly by 50% as well, resulting in fewer reinforcing agents in the CNT/GNP-Epoxy sample. Since CNTs and

Table 4
Sources and value of the normalized critical stress intensity factors, K_{IC}, of reinforced epoxies obtained from the literature and plotted in Fig. 1.

Author(s)	Material system	Nanoparticle weight concentration (%)	Normalized K_{IC}
Sun et al. (2007)	Epoxy-Pristine SWCNTs	1	1.035
	Epoxy-Functionalized SWCNTs (ammonia)	1	1.17
Chatterjee et al. (2012)	CNT-Epoxy	0.5	1.8
	25 μm GNP-Epoxy	0.5	1.6
	1:9 CNT:GNP-Epoxy	0.5	1.46
	9:1 CNT:GNP-Epoxy	0.5	1.79
	1:5 CNT:GNP-Epoxy	0.5	1.24
	5:1 CNT:GNP-Epoxy	0.5	1.46
	1:3 CNT-GNP-Epoxy	0.5	1.7
	3:1 CNT:GNP-Epoxy	0.5	1.7
Chatterjee et al. (2012)	5 μm GNP-Epoxy	0.1, 1, 2	1.02, 1.22, 1.59
	25 μm GNP-Epoxy	0.1, 1, 2	1.52, 1.7, 1.8
Ahmadi-Mohgadum et al. (2014)	25 μm GNP-Epoxy	0.5, 1, 2	1.24, 1.37, 1.68
	2:3 (25 μm GNP):CNT-Epoxy	0.5	1.32
	7:3 GNP-CNT-Epoxy	1	1.62
	1.7:0.3 GNP-CNT-Epoxy	2	1.75
Hernandez-Perez et al. (2007)	CNT-Epoxy	1	1.33
Zaman et al. (2011)	GNP-Epoxy	0.25, 1, 4	1.42, 1.08, 1.91
Ayatollahi et al. (2010)	MWCNT-Epoxy	0.1, 0.5, 1	1.15, 1.263, 1.192
Zhou et al. (2007)	CNT-Epoxy	0.1, 0.2, 0.3, 0.4	1.17, 1.25, 1.32, 1.07
Shokrieh et al. (2014)	GNP-Epoxy	0.5	1.152
Hsieh et al. (2011)	MWCNT-Epoxy	0.1, 0.2, 0.5	1.23, 1.25, 1.42
Rafiee et al. (2009)	SWCNT-Epoxy	0.1	1.12
	MWCNT-Epoxy	0.1	1.18
	GPL-Epoxy	0.1	1.467
Gojny et al. (2005)	Epoxy-SWCNT	0.05, 0.1, 0.3	1.1, 1.23, 1.12
	Epoxy-DWCNT	0.1, 0.3, 0.5	1.169, 1.30, 1.30
	Epoxy-MWCNT	0.1, 0.3	1.215, 1.23
Kumar et al.	GNP-Epoxy	0.1, 0.5	2.42, 3
Cha et al. (2017)	Melamine-CNT-Epoxy	1, 2, 3	1.98, 1.95, 2.02
	CNT-Epoxy	0.5, 1, 2, 3	1.4, 1.3, 1.45, 1.51
Zeinedini et al. (2018)	CNT-Epoxy	0.1, 0.3, 0.5, 0.7	1.085, 1.13, 1.24, 1.21
Cha et al. (2019)	GNP-Epoxy	2	1.49
	Melamine-GNP-Epoxy	2	2.25
Bisht et al. (2017)	GNP-Epoxy	0.1, 0.2, 0.3, 0.5, 1	1.4, 1.8, 2, 1.92, 1.32
	CNT-EPoxy	0.1, 0.2, 0.3, 0.5, 1	1.64, 2, 2.28, 2.48, 1.44
Domun et al. (2017)	Nitric Acid Functionalized GNP-Epoxy	0.1, 0.25, 0.5, 0.75, 1	1.32, 1.51, 1.4, 1.265, 1.135

GNPs, as individual nanofillers, have comparable stiffness, a reduction in the total number of stiffening/reinforcing agents in the epoxy can affect the local stiffness of the CNT/GNP-Epoxy regions. Therefore, it is not surprising that a CNT/GNP-Epoxy sample underperforms compared with the CNT-Epoxy counterpart. However, the same argument would suggest that a CNT/GNP-Epoxy sample should show a more significant enhancement compared with the GNP-Epoxy counterpart at the same nanofiller weight fraction. This is inconsistent with the experimental results presented here, which show that the CNT/GNP-Epoxy nanocomposites are only slightly outperformed by both CNT-Epoxy and GNP-Epoxy nanocomposites at a given nanofiller weight concentration. This observation suggests that other factors beyond the number of reinforcing elements are at work, such as the agglomeration behavior between CNTs and GNPs. This observation also suggests that 1:1 may not be the optimum ratio for CNT/GNP-Epoxy nanocomposites, although a significant enhancement in fracture toughness and fracture energy is still observed compared with neat epoxy. Further explorations are warranted to better understand the toughening mechanisms behind crack initiation and propagation in CNT and GNP reinforced epoxies and evaluate their effect on overall fracture toughness; and to elucidate the possible synergy between CNTs and GNPs as dual nanofillers.

4. Conclusions

In this study, enhancements in initiation fracture toughness of structural epoxies brought about by the addition of carbon nanotubes (CNTs) and graphene nanoplatelets (GNPS) have been investigated. Samples with different weight concentrations of nanofillers were studied and dual-nanofiller reinforcements were also explored to understand any synergistic effects that may exist between the two nanofillers. CNT-Epoxy, GNP-Epoxy, and CNT/GNP-Epoxy compact tension samples at 0.1% and 0.5% nanofiller weight concentrations were fabricated and tested according to ASTM D5045. Results were compared with those from neat Epoxy samples, which served as a baseline. Significant enhancements in critical stress intensity factor (K_{IC}) and critical fracture energy (G_{IC}) were observed in all samples. CNT-Epoxy samples at 0.5% weight concentration achieved the highest enhancement with a ~118% (1.64 MPa $\cdot\sqrt{\text{m}}$) and a ~103% (502.92 J/m^2) increase in K_{IC} and G_{IC}, respectively.

In the present study, there is a difference in the number of individual nanofillers dispersed in the matrix at the same weight concentration, as a result of the difference between the CNT and GNP particle sizes; more individual CNTs are present, compared to GNPs. This difference in number of nanofillers manifests itself by creating local nanofiller-matrix regions with a different stiffness for different nanocomposites. Local high stiffness regions in the matrix ahead of the crack tip, created by the addition of nanofillers, influence the size of the fracture process zone which is thought to be the primary cause for initiation toughness enhancement. Via scanning electron microscopy (SEM), crack bridging was found to be the dominant toughening mechanism for the CNT-Epoxy samples during crack propagation, where instances of CNT pullouts were regularly observed at the fractured surface. For the GNP-Epoxy samples, fractographical analysis revealed increased surface roughness, which could be considered as a marker of crack deflection. SEM images of the fractured surfaces in the CNT/GNP-Epoxy samples indicated the presence of CNT-rich regions, CNT pullouts, and increased surface roughness along with instances of crack bifurcations, suggesting that both crack bridging and crack deflection were at work during crack propagation.

At the 1:1 ratio of CNT:GNP, the CNT/GNP-Epoxy samples also show significant enhancements in their fracture properties compared with the neat epoxy. However, the enhancements are slightly weaker

than those in the CNT-Epoxy and GNP-Epoxy samples at the same wt% of the nanofillers. In other words, no synergy was found between CNTs and GNPs with regard to reinforcing epoxy polymers. This is likely due to the largely differing sizes of the CNTs and GNPs used in the present study, which may require a much different CNT:GNP ratio than 1:1. The results obtained highlight the complexity of fracture toughening mechanisms and the multitude of factors contributing to toughening, including particle size and shape, dispersion quality, the aspect ratio of nanofillers, their orientation, weight concentration, properties of the nanofiller itself, as well as the possible synergistic interactions in the case of multi-filler systems.

CRediT authorship contribution statement

Nishant Shirodkar: Methodology, Validation, Investigation, Writing – original draft, Visualization. **Shengfeng Cheng:** Project Administration, Funding acquisition, Writing – review & editing. **Gary D. Seidel:** Conceptualization, Supervision, Project administration, Funding acquisition, Writing – review & editing.

Declaration of competing interest

The authors declare that they have no known competing financial interests or personal relationships that could have appeared to influence the work reported in this paper.

Acknowledgments

The authors acknowledge the support of the Air Force Office of Scientific Research (AFOSR), USA Grant: FA9550-18-1-0433. The authors also acknowledge Virginia Tech's Nanoscale Characterization and Fabrication Lab (NCFL) for providing SEM imaging facilities.

Appendix

See Table 4.

References

[1] Miller EE, Hua Y, Tezel FH. Materials for energy storage: Review of electrode materials and methods of increasing capacitance for supercapacitors. J Energy Storage 2018;20(September):30–40. http://dx.doi.org/10.1016/j.est.2018.08.009.

[2] Mittal G, Dhand V, Rhee KY, Park SJ, Lee WR. A review on carbon nanotubes and graphene as fillers in reinforced polymer nanocomposites. J Ind Eng Chem 2015;21:11–25. http://dx.doi.org/10.1016/j.jiec.2014.03.022.

[3] Hofmann DC, Suh JY, Wiest A, Duan G, Lind ML, Demetriou MD, et al. Designing metallic glass matrix composites with high toughness and tensile ductility. Nature 2008;451(7182):1085–9. http://dx.doi.org/10.1038/nature06598.

[4] Argon AS, Cohen RE, Mower TM. Mechanisms of toughening brittle polymers. Mater Sci Eng A 1994;176(1–2):79–90. http://dx.doi.org/10.1016/0921-5093(94)90961-X.

[5] Domun N, Hadavinia H, Zhang T, Sainsbury T, Liaghat GH, Vahid S. Improving the fracture toughness and the strength of epoxy using nanomaterials-a review of the current status. Nanoscale 2015;7(23):10294–329. http://dx.doi.org/10.1039/c5nr01354b.

[6] Gojny FH, Wichmann MHG, Fiedler B, Schulte K. Influence of different carbon nanotubes on the mechanical properties of epoxy matrix composites - A comparative study. Compos Sci Technol 2005;65(15-16 SPEC. ISS.):2300–13. http://dx.doi.org/10.1016/j.compscitech.2005.04.021.

[7] Rosso P, Ye L, Friedrich K, Sprenger S. A toughened epoxy resin by silica nanoparticle reinforcement. J Appl Polym Sci 2006;100(3):1849–55. http://dx.doi.org/10.1002/app.22805.

[8] Gkikas G, Barkoula NM, Paipetis AS. Effect of dispersion conditions on the thermo-mechanical and toughness properties of multi walled carbon nanotubes-reinforced epoxy. Composites B 2012;43(6):2697–705. http://dx.doi.org/10.1016/j.compositesb.2012.01.070.

[9] Ravandi M, Teo WS, Tran LQN, Yong MS, Tay TE. The effects of through-the-thickness stitching on the Mode I interlaminar fracture toughness of flax/epoxy composite laminates. Mater Des 2016;109:659–69. http://dx.doi.org/10.1016/j.matdes.2016.07.093.

[10] Nuruzzaman DM. Composites communication. 2020, http://dx.doi.org/10.1016/j.coco.2020.100423.

[11] Wicks SS, Wardle BL. Interlaminar fracture toughness of laminated woven composites reinforced with aligned nanoscale fibers: Mechanisms at the macro, micro, and nano scales. In: 54th AIAA/ASME/ASCE/AHS/ASC structures, structural dynamics, and materials conference. 2013, p. 1–9. http://dx.doi.org/10.2514/6.2013-1612.

[12] Sela N, Ishai O. Interlaminar fracture toughness and toughening of laminated composite materials: A review. Composites 1989;20(5):423–35. http://dx.doi.org/10.1016/0010-4361(89)90211-5.

[13] Truong HTX, Lagoudas DC, Ochoa OO, Lafdi K. Fracture toughness of fiber metal laminates: Carbon nanotube modified Ti-polymer-matrix composite interface. J Compos Mater 2014;48(22):2697–710. http://dx.doi.org/10.1177/0021998313501923.

[14] Kamar NT, Drzal LT, Lee A, Askeland P. Nanoscale toughening of carbon fiber reinforced/epoxy polymer composites (CFRPs) using a triblock copolymer. Polymer 2017;111:36–47. http://dx.doi.org/10.1016/j.polymer.2017.01.009.

[15] Bakar M, Djaider F. Effect of plasticizers content on the mechanical properties of unsaturated polyester resin. J Thermoplast Compos Mater 2007;20(1):53–64. http://dx.doi.org/10.1177/0892705707068820.

[16] Heng Z, Chen Y, Zou H, Liang M. Simultaneously enhanced tensile strength and fracture toughness of epoxy resins by a poly(ethylene oxide)-block-carboxyl terminated butadiene-acrylonitrile rubber dilock copolymer. RSC Adv 2015;5(53):42362–8. http://dx.doi.org/10.1039/c5ra05124j.

[17] Dadfar MR, Ghadami F. Effect of rubber modification on fracture toughness properties of glass reinforced hot cured epoxy composites. Mater Des 2013;47:16–20. http://dx.doi.org/10.1016/j.matdes.2012.12.035.

[18] Vieira MGA, Da Silva MA, Dos Santos LO, Beppu MM. Natural-based plasticizers and biopolymer films: A review. Eur Polym J 2011;47(3):254–63. http://dx.doi.org/10.1016/j.eurpolymj.2010.12.011.

[19] Van Oosterhout JT, Gilbert M. Interactions between PVC and binary or ternary blends of plasticizers. Part I. PVC/plasticizer compatibility. Polymer 2003;44(26):8081–94. http://dx.doi.org/10.1016/j.polymer.2003.09.065.

[20] Kumar A, Li S, Roy S, King JA, Odegard GM. Fracture properties of nanographene reinforced EPON 862 thermoset polymer system. Compos Sci Technol 2015;114:87–93. http://dx.doi.org/10.1016/j.compscitech.2015.04.008.

[21] Shirodkar N, Rocker S, Seidel GD. Strain and damage sensing of polymer bonded mock energetics via piezoresistivity from carbon nanotube networks. Smart Mater Struct 2019;28(10):104006. http://dx.doi.org/10.1088/1361-665x/ab3dcd.

[22] Chaurasia AK, Seidel GD. Computational micromechanics analysis of electron-hopping-induced conductive paths and associated macroscale piezoresistive response in carbon nanotube–polymer nanocomposites. J Intell Mater Syst Struct 2014;25(17):2141–64. http://dx.doi.org/10.1177/1045389X13517314.

[23] Chaurasia AK, Ren X, Seidel GD. Computational micromechanics analysis of electron hopping and interfacial damage induced piezoresistive response in carbon nanotube-polymer nanocomposites. Smart Mater Struct 2014;23(7):075023. http://dx.doi.org/10.1088/0964-1726/23/7/075023.

[24] Chaurasia AK, Seidel GD. Computational micromechanics analysis of electron hopping and interfacial damage induced piezoresistive response in carbon nanotube-polymer nanocomposites subjected to cyclic loading conditions. Eur J Mech A Solids 2017;64:112–30. http://dx.doi.org/10.1016/j.euromechsol.2017.02.002.

[25] Chaurasia AK, Rukangu AM, Philen MK, Seidel GD, Freeman EC. Evaluation of bending modulus of lipid bilayers using undulation and orientation analysis. Phys Rev E 2018;97. 032421.

[26] Chaurasia AK, Sengezer EC, Talamadupula KK, Povolny S, Seidel GD. Experimental characterization and computational modeling of deformation and damage sensing through the piezoresistive response of nanocomposite bonded surrogate energetic materials. J Multifunct Compos 2014;2(4):227–53.

[27] Domínguez-Rodríguez G, Tapia A, Seidel GD, Avilés F. Influence of structural defects on the electrical properties of carbon nanotubes and their polymer composites. Adv Energy Mater 2016;18(11):1897–905. http://dx.doi.org/10.1002/adem.201600116.

[28] Dominguez-Rodriguez G, Chaurasia AK, Seidel GD, Tapia A, Aviles F. Hierarchical multiscale modeling of the effect of carbon nanotube damage on the elastic properties of polymer nanocomposites. J Mech Mater Struct 2017;12(3):263–87.

[29] Ku-Herrera JJ, Avilés F, Seidel GD. Self-sensing of elastic strain, matrix yielding and plasticity in multiwall carbon nanotube/vinyl ester composites. Smart Mater Struct 2013;22(8):085003.

[30] Li Y, Seidel GD. Multiscale modeling of the effects of nanoscale load transfer on the effective elastic properties of unfunctionalized carbon nanotube–polyethylene nanocomposites. Modelling Simulation Mater Sci Eng 2014;22(2):025023.

[31] Li Y, Seidel GD. Multiscale modeling of functionalized interface effects on the effective elastic material properties of CNT–polyethylene nanocomposites. Comput Mater Sci 2015;107:216–34.

[32] Li Y, Seidel GD. Multiscale modeling of the interface effects in CNT-epoxy nanocomposites. Comput Mater Sci 2018;153:363–81.

[33] Oliva-Avilés AI, Avilés F, Sosa V, Seidel GD. Dielectrophoretic modeling of the dynamic carbon nanotube network formation in viscous media under alternating current electric fields. Carbon 2014;69:342–54. http://dx.doi.org/10.1016/j.carbon.2013.12.035.

[34] Prakash N, Seidel GD. Electromechanical peridynamics modeling of piezoresistive response of carbon nanotube nanocomposites. Comput Mater Sci 2016;113:154–70.

[35] Prakash N, Seidel GD. Computational electromechanical peridynamics modeling of strain and damage sensing in nanocomposite bonded explosive materials (NCBX). Eng Fract Mech 2017;177:180–202.

[36] Prakash N, Seidel GD. Effects of microscale damage evolution on piezoresistive sensing in nanocomposite bonded explosives under dynamic loading via electromechanical peridynamics. Modelling Simulation Mater Sci Eng 2018;26(1):015003.

[37] Ren X, Seidel GD. Computational micromechanics modeling of piezoresistivity in carbon nanotube–polymer nanocomposites. Compos Interfaces 2013;20(9):693–720.

[38] Ren X, Seidel GD. Computational micromechanics modeling of inherent piezoresistivity in carbon nanotube–polymer nanocomposites. *J Intell Mater Syst Struct* 24(12):1459–83.

[39] Ren X, Burton J, Seidel GD, Lafdi K. Computational multiscale modeling and characterization of piezoresistivity in fuzzy fiber reinforced polymer composites. Int J Solids Struct 2015;54:121–34.

[40] Ren X, Chaurasia AK, Oliva-Avilés AI, Ku-Herrera JJ, Seidel GD, Avilés F. Modeling of mesoscale dispersion effect on the piezoresistivity of carbon nanotube-polymer nanocomposites via 3D computational multiscale micromechanics methods. Smart Mater Struct 2015;24(6):065031.

[41] Ren X, Chaurasia AK, Seidel GD. Concurrent multiscale modeling of coupling between continuum damage and piezoresistivity in CNT-polymer nanocomposites. Int J Solids Struct 2016;96:340–54. http://dx.doi.org/10.1016/j.ijsolstr.2016.05.018.

[42] Seifert R, Patil M, Seidel G, Reich G. Multifunctional topology optimization of strain-sensing nanocomposite beam structures. Struct Multidiscip Optim 2019;60(4):1407–22.

[43] Seifert R, Patil M, Seidel G. Topology optimization of self-sensing nanocomposite structures with designed boundary conditions. Smart Mater Struct 2019;28(7):074006 – 74014 pgs.

[44] Sengezer EC, Seidel GD, Bodnar RJ. Phenomenological characterization of fabrication of aligned pristine-SWNT and COOH-SWNT nanocomposites via dielectrophoresis under AC electric field. Polym Compos 2015;36(7):1266–79.

[45] Sengezer EC, Seidel GD, Bodnar RJ. Anisotropic piezoresistivity characteristics of aligned carbon nanotube-polymer nanocomposites. Smart Mater Struct 2017;26(9):095027. http://dx.doi.org/10.1088/1361-665x/aa78c3.

[46] Sengezer EC, Seidel GD. Structural health monitoring of nanocomposite bonded energetic materials through piezoresistive response. AIAA J 2018;56(3):1225–38.

[47] Talamadupula KK, Povolny SJ, Prakash N, Seidel GD. Mesoscale strain and damage sensing in nanocomposite bonded energetic materials under low velocity impact with frictional heating via peridynamics. Modelling Simulation Mater Sci Eng 2020;28(8):085011.

[48] Talamadupula KK, Povolny SJ, Prakash N, Seidel GD. Piezoresistive detection of simulated hotspots and the effects of low velocity impact at the mesoscale in nanocomposite bonded energetic materials via multiphysics peridynamics modeling. Comput Mater Sci 2021;188:110211–30.

[49] Sun L, Warren GL, O'Reilly JY, Everett WN, Lee SM, Davis D, et al. Mechanical properties of surface-functionalized SWCNT/epoxy composites. Carbon 2008;46(2):320–8. http://dx.doi.org/10.1016/j.carbon.2007.11.051.

[50] Wang F, Drzal LT, Qin Y, Huang Z. Size effect of graphene nanoplatelets on the morphology and mechanical behavior of glass fiber/epoxy composites. J Mater Sci 2016;51(7):3337–48. http://dx.doi.org/10.1007/s10853-015-9649-x.

[51] Zhou Y, Pervin F, Lewis L, Jeelani S. Fabrication and characterization of carbon/epoxy composites mixed with multi-walled carbon nanotubes. Mater Sci Eng A 2008;475(1–2):157–65. http://dx.doi.org/10.1016/j.msea.2007.04.043.

[52] Hsieh TH, Kinloch AJ, Taylor AC, Kinloch IA. The effect of carbon nanotubes on the fracture toughness and fatigue performance of a thermosetting epoxy polym. J Mater Sci 2011;46(23):7525–35. http://dx.doi.org/10.1007/s10853-011-5724-0.

[53] Zaman I, Phan TT, Kuan HC, Meng Q, Bao La LT, Luong L, et al. Epoxy/graphene platelets nanocomposites with two levels of interface strength. Polymer 2011;52(7):1603–11. http://dx.doi.org/10.1016/j.polymer.2011.02.003.

[54] Rafiee MA, Rafiee J, Wang Z, Song H, Yu ZZ, Koratkar N. Enhanced mechanical properties of nanocomposites at low graphene content. ACS Nano 2009;3(12):3884–90. http://dx.doi.org/10.1021/nn9010472.

[55] Shokrieh MM, Ghoreishi SM, Esmkhani M, Zhao Z. Effects of graphene nanoplatelets and graphene nanosheets on fracture toughness of epoxy nanocomposites. Fatigue Fract Eng Mater Struct 2014;37(10):1116–23. http://dx.doi.org/10.1111/ffe.12191.

[56] Ayatollahi MR, Shadlou S, Shokrieh MM. Fracture toughness of epoxy/multi-walled carbon nanotube nano-composites under bending and shear loading conditions. Mater Des 2011;32(4):2115–24. http://dx.doi.org/10.1016/j.matdes.2010.11.034.

[57] Chatterjee S, Nafezarefi F, Tai NH, Schlagenhauf L, Nüesch FA, Chu BTT. Size and synergy effects of nanofiller hybrids including graphene nanoplatelets and carbon nanotubes in mechanical properties of epoxy composites. Carbon 2012;50(15):5380–6. http://dx.doi.org/10.1016/j.carbon.2012.07.021.

[58] Ahmadi-Moghadam B, Taheri F. Fracture and toughening mechanisms of GNP-based nanocomposites in modes I and II fracture. Eng Fract Mech 2014;131:329–39. http://dx.doi.org/10.1016/j.engfracmech.2014.08.008.

[59] Hernández-Pérez A, Avilés F, May-Pat A, Valadez-González A, Herrera-Franco PJ, Bartolo-Pérez P. Effective properties of multiwalled carbon nanotube/epoxy composites using two different tubes. Compos Sci Technol 2008;68(6):1422–31. http://dx.doi.org/10.1016/j.compscitech.2007.11.001.

[60] Cha J, Jun GH, Park JK, Kim JC, Ryu HJ, Hong SH. Improvement of modulus, strength and fracture toughness of CNT/Epoxy nanocomposites through the functionalization of carbon nanotubes. Composites B 2017;129:169–79. http://dx.doi.org/10.1016/j.compositesb.2017.07.070.

[61] Cha J, Kim J, Ryu S, Hong SH. Comparison to mechanical properties of epoxy nanocomposites reinforced by functionalized carbon nanotubes and graphene nanoplatelets. Composites B 2019;162(July 2018):283–8. http://dx.doi.org/10.1016/j.compositesb.2018.11.011.

[62] Bisht A, Dasgupta K, Lahiri D. Effect of graphene and CNT reinforcement on mechanical and thermomechanical behavior of epoxy—A comparative study. J Appl Polym Sci 2018;135(14):1–11. http://dx.doi.org/10.1002/app.46101.

[63] Domun N, Paton KR, Hadavinia H, Sainsbury T, Zhang T, Mohamud H. Enhancement of fracture toughness of epoxy nanocomposites by combining nanotubes and nanosheets as fillers. Materials 2017;10(10). http://dx.doi.org/10.3390/ma10101179.

[64] Zeinedini A, Shokrieh MM, Ebrahimi A. The effect of agglomeration on the fracture toughness of CNTs-reinforced nanocomposites. Theor Appl Fract Mech 2018;94(November 2017):84–94. http://dx.doi.org/10.1016/j.tafmec.2018.01.009.

[65] ASTM International. (ASTM D 5054) - Standard test methods for plane-strain fracture toughness and strain energy release rate of plastic materials. In: ASTM book of standards, vol. 99, (Reapproved 2007):2013, p. 1–9, http://www.astm.org/cgi-bin/resolver.cgi?D5045-14.

[66] ISO 13586:2000. Plastic – Determination of fracture toughness (GIC and KIC) – Linear elastic fracture mechanics (LEFM) approach. 2000-03, 61010-1 © Iec:2001. 1:16.

[67] EPIKOTE H. [DATASHEET] EPIKOTE Resin 862/EPIKURE curing agent W system. 2016, p. 1–11, https://www.miller-stephenson.com/wp-content/uploads/2016/08/W.pdf.

[68] Quaresimin M, Schulte K, Zappalorto M, Chandrasekaran S. Toughening mechanisms in polymer nanocomposites: From experiments to modelling. Compos Sci Technol 2016;123(October 2017):187–204.

[69] Chandrasekaran S, Sato N, Tölle F, Mülhaupt R, Fiedler B, Schulte K. Fracture toughness and failure mechanism of graphene based epoxy composites. Compos Sci Technol 2014;97:90–9. http://dx.doi.org/10.1016/j.compscitech.2014.03.014.

[70] Gdoutos EE. Fracture mechanics. vol. 123. Springer; 2005, http://dx.doi.org/10.1007/1-4020-3153-X.

[71] Huang Y, Kinloch AJ. Modelling of the toughening mechanisms in rubber-modified epoxy polymers - Part I finite element analysis studies. J Mater Sci 1992;27(10):2753–62. http://dx.doi.org/10.1007/BF00540702.

[72] Chatterjee S, Nafezarefi F, Tai NH, Schlagenhauf L, Nüesch FA, Chu BTT. Size and synergy effects of nanofiller hybrids including graphene nanoplatelets and carbon nanotubes in mechanical properties of epoxy composites. Carbon 2012;50(15):5380–6. http://dx.doi.org/10.1016/j.carbon.2012.07.021.

[73] Liu Y, Ramirez C, Zhang L, Wu W, Padture NP. In situ direct observation of toughening in isotropic nanocomposites of alumina ceramic and multiwall carbon nanotubes. Acta Mater 2017;127:203–10. http://dx.doi.org/10.1016/j.actamat.2017.01.024.

[74] Wang PH, Sarkar S, Gulgunje P, Verghese N, Kumar S. Fracture mechanism of high impact strength polypropylene containing carbon nanotubes. Polymer 2018;151:287–98. http://dx.doi.org/10.1016/j.polymer.2018.07.031.

[75] Opelt CV, Becker D, Lepienski CM, Coelho LAF. Reinforcement and toughening mechanisms in polymer nanocomposites - Carbon nanotubes and aluminum oxide. Composites B 2015;75:119–26. http://dx.doi.org/10.1016/j.compositesb.2015.01.019.

[76] Liu Q, Lomov SV, Gorbatikh L. The interplay between multiple toughening mechanisms in nanocomposites with spatially distributed and oriented carbon nanotubes as revealed by dual-scale simulations. Carbon 2019;142:141–9. http://dx.doi.org/10.1016/j.carbon.2018.10.005.

[77] Li M, Tsujimura M, Sakai M. Crack-face grain interlocking/bridging of a polycrystalline graphite: The role in mixed mode fracture. Carbon 1999;37(10):1633–9. http://dx.doi.org/10.1016/S0008-6223(99)00026-3.

[78] Cui S, Lu Z, Yang Z. Effect of interlocking structure on mechanical properties of bio-inspired nacreous composites. Compos Struct 2019;226(July):111260. http://dx.doi.org/10.1016/j.compstruct.2019.111260.

[79] Liu Q, Lomov SV, Gorbatikh L. The interplay between multiple toughening mechanisms in nanocomposites with spatially distributed and oriented carbon nanotubes as revealed by dual-scale simulations. Carbon 2019;142:141–9. http://dx.doi.org/10.1016/j.carbon.2018.10.005.